



Cite this: *Org. Biomol. Chem.*, 2016, **14**, 4089

## Structural and morphological diversity of self-assembled synthetic $\gamma$ -amino acid containing peptides†

Maruthi Konda,<sup>a</sup> Brice Kauffmann,<sup>b</sup> Dnyaneshwar B. Rasale<sup>a</sup> and Apurba K. Das<sup>\*a</sup>

Regulating the nanostructural morphology of synthetic hybrid peptides through external stimuli is still a great challenge. Here, we report the synthesis of constrained amino acid building block gabapentin (Gpn) based hybrid peptides and their structural and morphological diversity in different conditions. The synthesized three hybrid peptides Boc-Gpn-Aib-Phe-Aib-OMe (**P1**), Boc-Gpn-Aib-Leu-Aib-OMe (**P2**) and Boc-Gpn-Aib-Tyr-Aib-OMe (**P3**) are folded into  $C_{12}/C_{10}$  hydrogen-bonded double turn conformations. The double turn feature is probed and confirmed by conformational analysis of hybrid peptides using 2D-NMR studies and X-ray crystallography. DMSO- $d_6$  solvent titration investigations also support the double turn conformation adopted by our reported peptides in  $CDCl_3$  solution. Solvent assisted self-assembled morphological features of peptides **P1–P3** and the salt-prompted mineralization studies of peptide **P1** under ambient conditions are studied. All three reported peptides **P1–P3** form diverse supramolecular scaffolds in solid states through non-covalent interactions to attain higher order architectures.

Received 17th February 2016.

Accepted 24th March 2016

DOI: 10.1039/c6ob00380j

www.rsc.org/obc

## Introduction

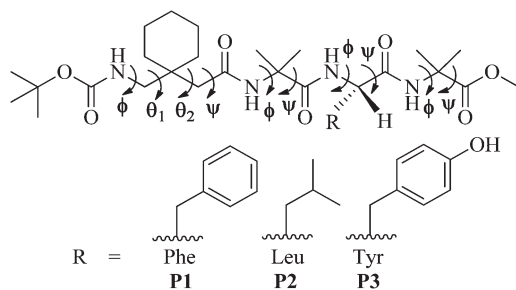
Molecular self-assembly of small organic molecules has attracted considerable interest in recent years due to its applications in biology and material sciences. Biomolecular self-assembly is spontaneous and reversible which is governed by the combination of various covalent and non-covalent interactions. Molecular self-assembly facilitates the organization of small organic molecules into higher order functional nanostructures. Peptide self-assembly offers significant advantages due to its biological compatibility, ease of synthesis, low toxicity and multi-functionalibility.<sup>1</sup> Strategies to design and control supramolecular architectures are important as the properties of a material are associated with the molecular structure of self-assembling building blocks. Peptides are an attractive scaffold for this task. Natural amino acid based peptide scaffolds for the development of supramolecular architectures have limitations due to their proteolytic hydrolysis.<sup>2</sup>

There is an increased interest for modular synthesis of unnatural amino acids for designing amphiphilic self-assembling peptide scaffolds. In nature, proteins/peptides are made up of natural amino acids, which have the tendency to fold into regular secondary structures such as helices, sheets and turns. In living systems, peptides show specific and important biochemical tasks because of their compact folded conformations and self-assembly.<sup>3</sup> Small synthetic unnatural amino acids can be incorporated to mimic the secondary structural features of peptides<sup>4</sup> and to impart biological stability as well. Synthesis of  $\beta$  and  $\gamma$ -peptides has vast importance in medicinal chemistry owing to their resistant to the action of protease enzymes.<sup>5</sup> Therefore,  $\beta$  and  $\gamma$ -amino acids are being used to mimic the distinct self-assembled structure of peptides. At the same time diverse H-bonded folded structures are investigated *via* design and synthesis of various peptide sequences which evinced mimicry of discrete peptide secondary structures.<sup>6–8</sup> Short synthetic peptides are platforms to understand the folding patterns with numerous H-bonded conformational preferences.<sup>9</sup> Gabapentin, a constrained achiral  $\beta,\beta$ -disubstituted  $\gamma$ -amino acid and  $\alpha$ -amino isobutyric acid (Aib) are unnatural amino acids which enhance the helical turn behaviour of the peptide backbone. Various constrained cyclic  $\gamma$ -amino acids have been used to mimic the secondary structure in the solid state. Self-assembly of these peptides leads to the formation of sheet and ribbon type structures at their supramolecular level.<sup>10</sup> There are few reports on constrained aromatic  $\gamma$  and  $\delta$ -amino acids based peptides, which adopt double helices,<sup>11</sup>

<sup>a</sup>Department of Chemistry, Indian Institute of Technology Indore, Indore 452020, India. E-mail: apurba.das@iiti.ac.in

<sup>b</sup>Université de Bordeaux, UMS3033, Institut Européen de Chimie et Biologie (IECB), 2 rue Escarpit, 33600 Pessac, France

† Electronic supplementary information (ESI) available: Figures, tables, crystal and diffraction parameters, <sup>1</sup>H NMR, <sup>13</sup>C NMR, and HRMS mass spectra of all new compounds. X-ray data for **P1–P3** have been deposited with the Cambridge Crystallographic Data Centre. CCDC 1054010 for **P1**, 1463837 for **P2** and 1054011 for **P3**. For ESI and crystallographic data in CIF or other electronic format see DOI: 10.1039/c6ob00380j



**Scheme 1** Chemical structures of peptides P1, P2 and P3 with backbone torsion angles parameters.

helices<sup>12</sup> and extended sheets.<sup>13</sup> In particular, aromatic  $\gamma$ -hybrid peptides reveal different self-assembled nanostructures at the supramolecular level and possess various applications in nanotechnology.<sup>14</sup> However, several groups have designed and synthesized short hybrid peptides through a suitable choice of natural and synthetic building blocks which adopt interesting double turn/bent conformation.<sup>15–17</sup> Thus, there is considerable interest to study using short peptide based small molecules with intriguing H-bonded conformations. Here, our objectives are (i) to synthesize Gpn containing hybrid peptides with the sequence Boc-Gpn-Aib-Xaa-Aib-OMe (where Xaa = phenylalanine for P1, leucine for P2 and tyrosine for P3), differing in third residue side chains, (ii) to study the structural propensities of  $\gamma\alpha$ -hybrid peptides P1, P2, P3 in the solid state as well as in a solution state by means of substitution of the amino acid residue at the third position of the peptide sequence and (iii) to analyze distinct nanostructural morphological features of peptides in different solvents and conditions.

Herein, we report C<sub>12</sub>/C<sub>10</sub> hydrogen-bonded double turn conformations and diverse supramolecular propensities of three short peptides where Gpn is placed at the N-terminal of the peptide sequence and a variable amino acid residue (Phe or Leu or Tyr) is placed at the third position of the C-termini of the peptide sequence. The turn structures are observed in hybrid peptides containing conformationally constrained  $\gamma$ -amino acid *i.e.* gabapentin sequence of Boc-Gpn-Aib-Xaa-Aib-OMe (Scheme 1).

## Results and discussion

Conformationally constrained  $\beta,\beta$ -disubstituted  $\gamma$ -amino acid (Gpn)<sup>18</sup> and  $\alpha,\alpha$ -dialkylated residue  $\alpha$ -aminoisobutyric acid (Aib)<sup>19,20</sup> are well known as powerful inducers which can restrict the local accessible conformations and induce helicity and crystallinity to the peptide backbone. The available information allowed us to design hybrid peptides where the Boc-Gpn-Aib segment has been used as a constituent and the third position has been altered with proteinogenic aromatic/aliphatic amino acids. The C-termini of the synthesized peptide sequence is occupied by an Aib residue. We have synthesized three hybrid peptides Boc-Gpn-Aib-Phe-Aib-OMe (P1), Boc-

Gpn-Aib-Leu-Aib-OMe (P2), and Boc-Gpn-Aib-Tyr-Aib-OMe (P3) by conventional solution-phase methodology (Scheme S1†). Our investigations exemplified that the  $\gamma\alpha$ -peptides P1–P3 are explored to show diversity in self-assembly propensities in both solid and solution states. Phenylalanine in peptide P1 contains an aromatic side chain which can provide a platform for aromatic–aromatic and other non-covalent interactions. The third residue in peptide P2 is substituted by leucine, which has an aliphatic side chain. In peptide P3, tyrosine is used as a substituent at the third position of the peptide sequence, which has the capability to show aromatic–aromatic interactions along with side chain phenolic –OH functionality, an additional hydrogen bonding site.<sup>21</sup>

### NMR study

In the course of structural investigations of the reported hybrid peptides, we have first investigated the conformational preferences in CDCl<sub>3</sub> at 298 K. The comprehensive <sup>1</sup>H NMR spectrum assignments of three peptides have been achieved by using a combination of 2D COSY and ROESY experiments (Fig. S1–S5†). Table 1 summarizes the chemical shifts of several amide resonances for peptides P1, P2 and P3. The folded or turn conformation of peptides is stabilized by intra-molecular hydrogen-bonds. The intra-molecular hydrogen-bonds of peptides are favored in CDCl<sub>3</sub> which is a poorly interacting solvent with peptides and does not possess any strong hydrogen-bonding groups. The presence of intra-molecular hydrogen-bonded NH groups and the strength of the hydrogen-bonds are measured by a solvent titration study with a hydrogen-bond accepting solvent like DMSO-*d*<sub>6</sub> to the solution of peptides in CDCl<sub>3</sub>. The effect of DMSO-*d*<sub>6</sub> addition to the solution of peptides P1, P2 and P3 is represented in Fig. 1. Generally, the addition of a small amount of DMSO-*d*<sub>6</sub> to the CDCl<sub>3</sub> solution of peptides can shift the chemical shift to a downfield region for the solvent exposed NH groups. There is a negligible change in the chemical shift for strong hydrogen-bonded or solvent shielded NH groups.

Fig. 1 reveals the shielded nature of the NH groups of Aib(4), Phe(3) and Aib(2) for peptide P1, Aib(4) NH, Leu(3) NH and Aib(2) NH for peptide P2, and Aib(4) NH, Tyr(3) NH and Aib(2) NH for peptide P3. By addition of DMSO-*d*<sub>6</sub> to the peptide solution in CDCl<sub>3</sub>, a very minor solvent dependence behavior was observed for the three NHs except Gpn NH. In

**Table 1** Representative <sup>1</sup>H NMR NH resonances observed for peptides P1, P2 and P3 (Chemical shifts  $\delta^a$ )

Residue	P1 $\delta$ ppm	$\Delta\delta^b$	P2 $\delta$ ppm	$\Delta\delta^b$	P3 $\delta$ ppm	$\Delta\delta^b$
Gpn (1) NH	5.98(4.89)	1.09	5.96(4.82)	1.14	6.05(4.91)	1.14
Aib (2) NH	8.09(7.98)	0.11	8.00(7.76)	0.24	8.20(8.00)	0.20
Xaa <sup>c</sup> (3) NH	6.79(6.36)	0.43	6.95(6.53)	0.42	6.65(6.37)	0.28
Aib (4) NH	7.36(7.56)	0.20	7.57(7.33)	0.24	7.63(7.30)	0.33

<sup>a</sup> Chemical shifts of proton resonances in 8% DMSO-*d*<sub>6</sub>/CDCl<sub>3</sub>, values in parentheses correspond to CDCl<sub>3</sub>. <sup>b</sup>  $\Delta\delta$  is the chemical shift difference for NH protons in 8% DMSO-*d*<sub>6</sub>/CDCl<sub>3</sub> and CDCl<sub>3</sub>. <sup>c</sup> Xaa(3) = Phe (3) for P1, = Leu (3) for P2, = Tyr (3) for P3.

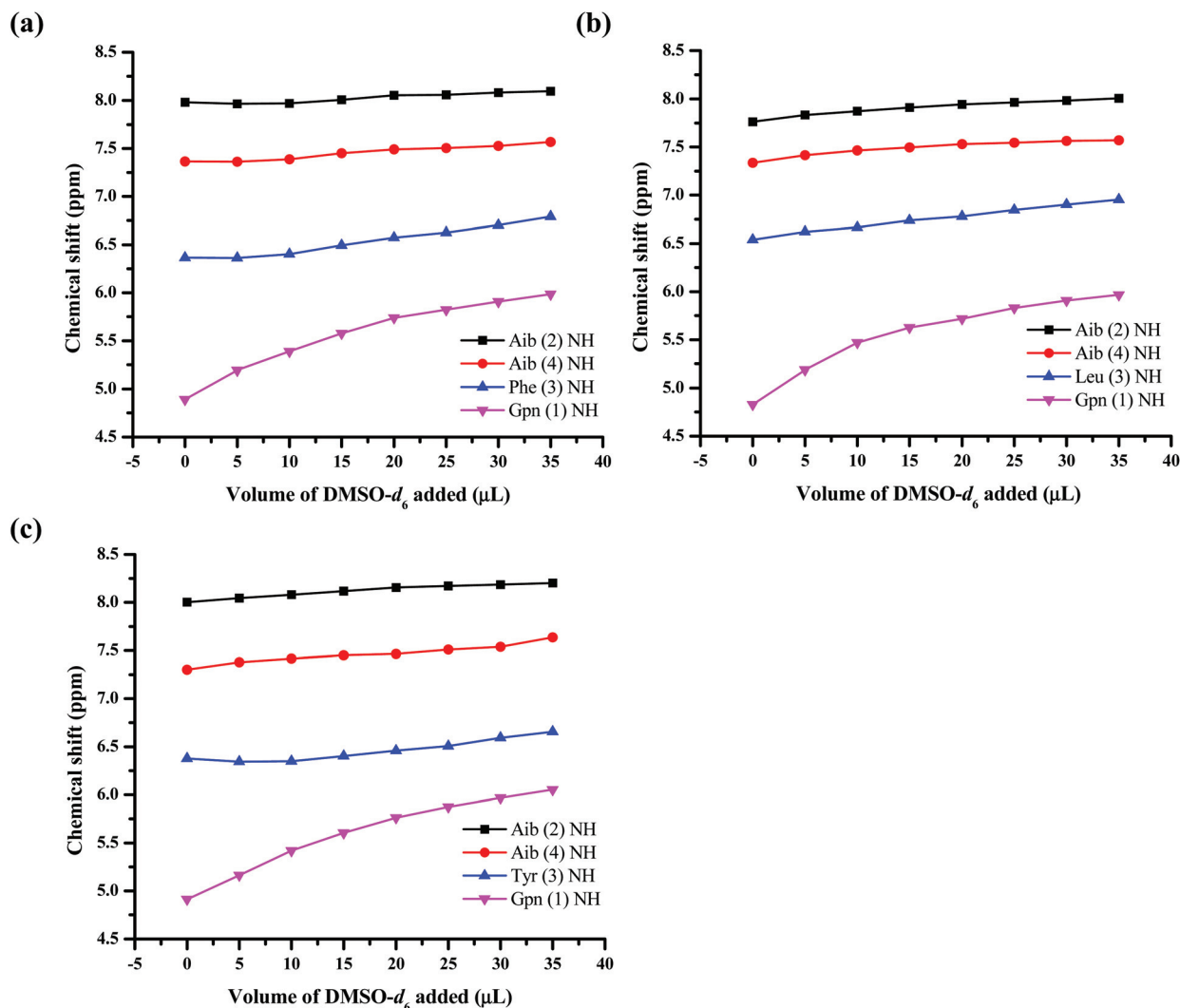


Fig. 1 DMSO-*d*<sub>6</sub> solvent titration plots for peptides (a) P1, (b) P2, (c) P3 in CDCl<sub>3</sub>. The initial concentration of the samples in CDCl<sub>3</sub> was 20 mmol L<sup>-1</sup>, and the total amount of DMSO-*d*<sub>6</sub> used was 8% of the total volume.

contrast, Gpn(1) NHs of peptides P1, P2 and P3 show solvent sensitivity with a downfield shift upon addition of DMSO-*d*<sub>6</sub>. Solvent insensitivity behavior appeared for several solvent shielded NH groups of peptides P1–P3 which was supported by the observation of small values of  $\Delta\delta_{\text{NH}} < 0.45$  ppm ( $\delta_{(\text{CDCl}_3+8.00\% \text{ DMSO-}d_6)} - \delta_{(\text{CDCl}_3)}$ ), ppm, Table 1). These results suggest that Aib(2) NH, Phe(3) NH and Aib(4) NH for peptide P1, Aib(2) NH, Leu(3) NH and Aib(4) NH for peptide P2 and Aib(2) NH, Tyr(3) NH and Aib(4) NH for peptide P3 are involved in hydrogen-bonding interactions.<sup>7a,b</sup>

To know about the inter-residue NOEs, ROESY experiments were carried out in CDCl<sub>3</sub>. Fig. S2 and S5† show ROESY spectra of peptides P1 and P3 in CDCl<sub>3</sub>. Various inter-residual NOEs for P1 and P3 are listed in Table S1.† The ROESY spectrum of P1 reveals some important NOEs that are observed between backbone NH protons. In the ROESY spectrum of P1, the  $d_{\text{NN}[(i)\leftrightarrow(i+1)]}$  and  $d_{\alpha\text{N}[(i)\leftrightarrow(i+1)]}$  medium range NOEs are perceived over the peptide backbone. The scrutiny of  $d_{\text{NN}[(i)\leftrightarrow(i+1)]}$

NOEs of Aib(2) NH  $\leftrightarrow$  Phe(3) NH and Phe(3) NH  $\leftrightarrow$  Aib(4) NH along with  $d_{\alpha\text{N}[(i)\leftrightarrow(i+1)]}$  NOEs Phe(3) C<sup>α</sup>H  $\leftrightarrow$  Aib(4) NH is indicative of the presence of a turn conformation in solution. From the crystal structure of P1, inter proton  $d_{\text{NN}}$  distances observed in the double turn conformation between Aib(2) NH  $\leftrightarrow$  Phe(3) NH and Phe(3) NH  $\leftrightarrow$  Aib(4) NH are 2.72 Å and 2.74 Å respectively. Some other NOEs between Aib(2) NH  $\leftrightarrow$  Gpn(1) C<sup>α</sup>H and Aib(2) NH  $\leftrightarrow$  Aib(2) C<sup>β</sup>H are also observed. In the DMSO-*d*<sub>6</sub> titration experiment, the  $\Delta\delta_{\text{NH}}$  values are observed as 1.09 ppm for Gpn(1) NH, 0.11 ppm for Aib(2) NH, 0.43 ppm for Phe(3) NH and 0.20 ppm for Aib(4) NH. The high  $\Delta\delta_{\text{NH}}$  value for Gpn(1) NH indicates the solvent exposed nature. The low  $\Delta\delta_{\text{NH}}$  values for the rest of the NH protons indicate the solvent-shielded behavior. The NOEs data and solvent-shielded nature of Phe(3) NH are supportive of a 12-membered hydrogen-bonded ring conformation between (Boc)C=O and H–N of Phe(3). In peptide P1, the observations of  $d_{\alpha\text{N}[(i)\leftrightarrow(i+1)]}$  medium range NOEs for Phe(3), Aib(4) and

$d_{\text{NN}[(i)\leftrightarrow(i+1)]}$  medium range NOEs for residues Aib(2), Phe(3) and Phe(3), Aib(4) distinctly suggest the presence of a 10-membered hydrogen-bond conformation ( $\beta$ -turn), which involves the interaction between Gpn(1) C=O and H-N Aib(4).

2D ROESY spectra of peptides P2 and P3 do not show several critical NOEs in  $\text{CDCl}_3$  at a mixing time of 200 ms. Though the DMSO- $d_6$  titration study reveals that  $\Delta\delta$  NH values are observed for P2 as 1.14 ppm for Gpn(1) NH, 0.24 ppm for Aib(2) NH, 0.42 ppm for Leu(3) NH and 0.24 ppm for Aib(4) NH. For peptide P3,  $\Delta\delta$  NH values are observed as 1.14 ppm for Gpn(1) NH, 0.20 ppm for Aib(2) NH, 0.28 ppm for Tyr(3) NH and 0.33 ppm for Aib(4) NH. The high  $\Delta\delta$  NH values for Gpn(1) NH for both peptides P2 and P3 elucidate the solvent exposed nature and the remaining NH protons show solvent shielded behavior. Some of the NOEs observed for peptide P3 are listed in Table S1.† The solvent-titration studies support that the peptides P2 and P3 are folded in a double turn conformation similarly to P1 in  $\text{CDCl}_3$ .

### Circular dichroism (CD) study

Circular dichroism is a useful tool to elucidate the propensity of conformational features of peptides in solution. Fig. 2 shows circular dichroism spectra of peptides P1, P2 and P3 in a methanol:water (1:1 v/v) solution and reveals a distinct pattern of Cotton effects. The CD spectrum of peptide P1 shows characteristic positive CD signatures at 193 nm and 196 nm (attributed to the  $\pi$ - $\pi^*$  transition) and negative CD signatures at 205 nm, 215 nm and 220 nm (attributed to the  $n$ - $\pi^*$  transition) which suggest a helical conformation. The CD spectrum of peptide P2 shows a positive CD signature at 190 nm (attributed to the  $\pi$ - $\pi^*$  transition) and a strong negative signature at 200 nm (attributed to the  $n$ - $\pi^*$  transition). This pattern of CD indicates the adaptation of a  $\beta$ -hairpin type of structure. The CD spectrum of peptide P3 shows a positive CD signature at 200 nm and a negative signature at 210 nm, which corres-

pond to the  $n$ - $\pi^*$  transition. Another negative CD band at 230 nm is also observed. The observed diagnostic CD signatures of peptide P3 can be assigned to the presence of a helical conformation. Peptides P1 and P3 show a similar type of CD pattern with small CD shifts while peptide P2 shows a completely different type of CD pattern. As peptides P1 and P3 contain an aromatic side-chain which contributes towards the overall CD of peptide secondary structures along with peptide chromophores, therefore the coupling interactions of the local band ( $L_a$  band) of the aromatic chromophore with backbone peptide groups and other nearby groups are found responsible for showing such Cotton effects. Peptide P2 has no aromatic chromophore and as such does not show such coupling interactions.<sup>22</sup>

### Morphological analysis of peptides

We observed interesting molecular self-assembly and nanostructural transformation of these hybrid peptides in solution as well as in solid states. Self-assembly phenomena of these peptides were observed by the involvement of various non-covalent interactions and, as a result, peptides can form various nanostructural features.<sup>23</sup> Peptide based self-assembled structures may have significant importance as bio-materials in bio-medicinal applications.<sup>24-26</sup> To investigate solvent assisted self-assembled morphological diversity of peptides P1-P3, we performed scanning and transmission electron microscopy to study the morphological features (Fig. 3-5). As shown in the SEM image (Fig. 3a), peptide P1 forms self-assembled microspheres in methanol:water (1:1) at a concentration of 3.0 mmol  $\text{L}^{-1}$ . These spherical entities have a diameter approximately ranging from 75 nm to 325 nm. The SEM image clearly depicts the presence of smaller and larger spherical aggregates. These larger spherical aggregates could be formed by the fusion of small spherical structures.<sup>27-29</sup> Transmission electron microscopy investigations were also performed to image the self-assembled morphological features. The TEM image (Fig. 3c) clearly shows well-organized self-assembled spherical entities. The average diameter of these spherical entities observed in TEM studies is found to be 143 nm. The TEM image also clearly shows the formation of larger spherical aggregates from relatively small spherical structures by a fusion process which has been similarly observed through SEM measurements (Fig. 3a). In addition to that, the formation of self-assembled spherical nanostructures in solution was also supported by a dynamic light scattering (DLS) experiment of peptide P1. DLS is a technique to measure size distribution of nanostructures in solution. The DLS study (Fig. S6†) revealed an average diameter of 201 nm for self-assembled spherical aggregates of peptide P1 ( $c = 3.0$  mmol  $\text{L}^{-1}$  in methanol-water (1:1) solution).<sup>14a,b,27a</sup> SEM and TEM results altogether evidenced the formation of self-assembled spherical aggregates by peptide P1 in a polar solvent (methanol-water (1:1) solution) which was also supported by DLS measurements. Surprisingly, SEM and TEM studies in a THF-water (1:1) solvent (Fig. 3b and d) of peptide P1 ( $c = 5$  mmol  $\text{L}^{-1}$ ) demonstrate the change in morphological features, which form exclusively nanorod assemblies under similar experi-

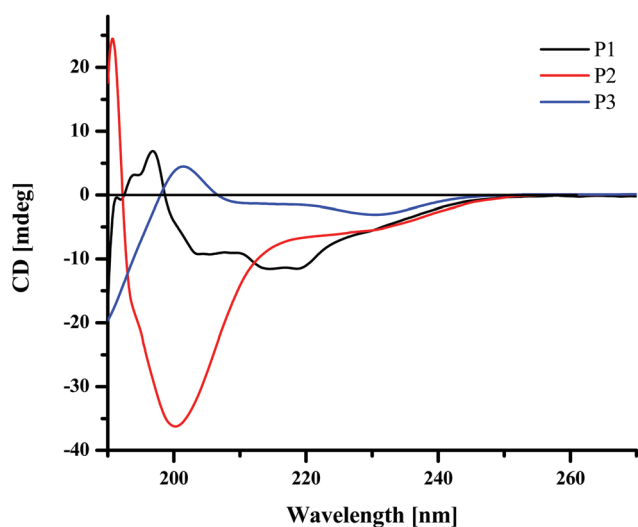
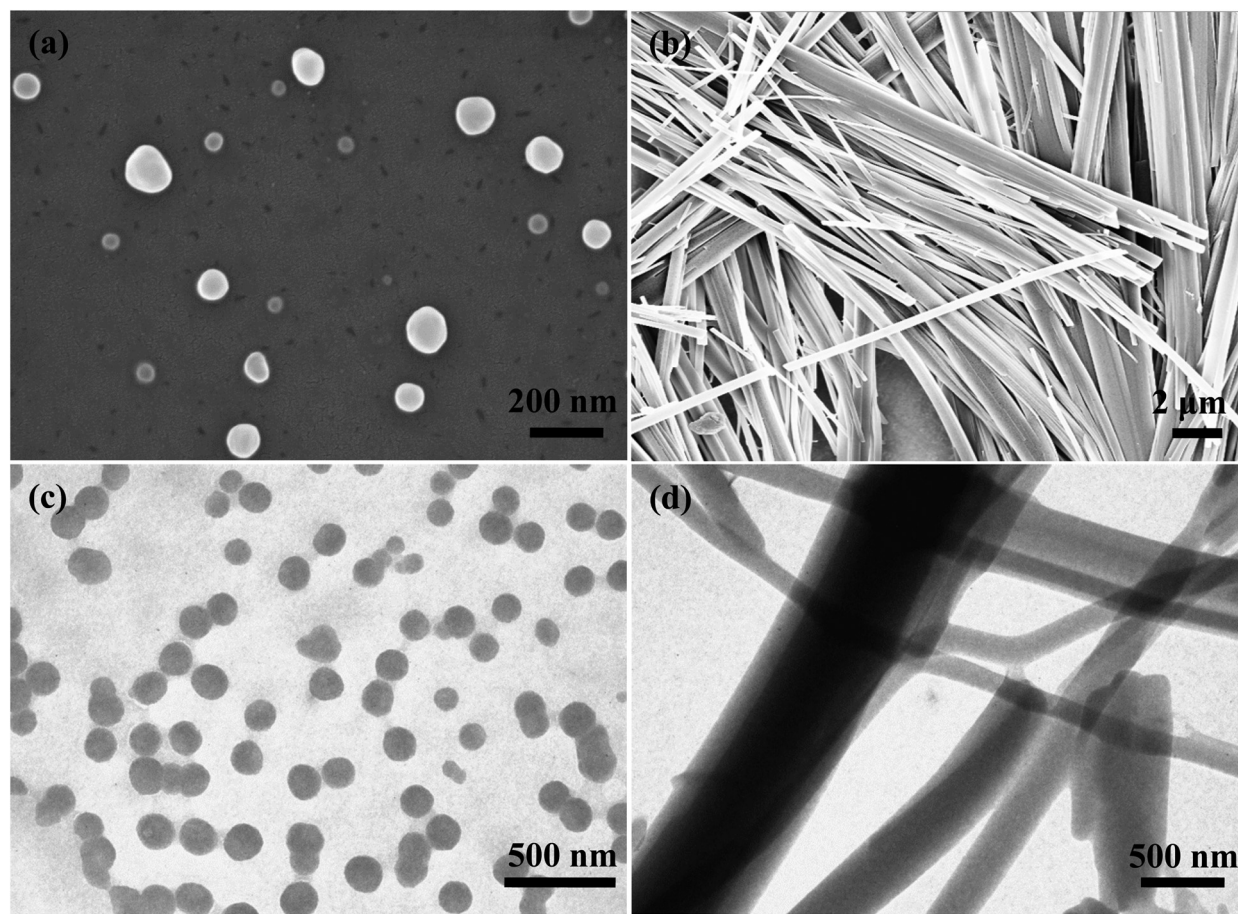
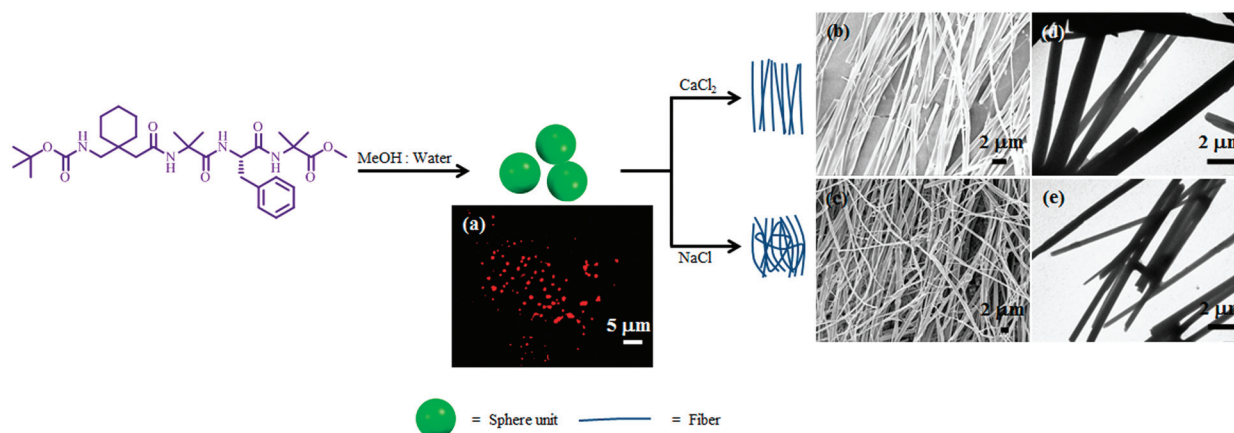


Fig. 2 Circular dichroism spectra of peptides P1, P2 and P3 in MeOH-water (1:1).  $C = 0.625$  mmol  $\text{L}^{-1}$  at 25 °C.



**Fig. 3** Electron microscopy analysis of the self-assembled structures formed by peptide P1 and showing the solvent assisted morphological diversity. Image (a) SEM and (c) TEM showing the well-organized spherical aggregates formed in a methanol–water (1 : 1 v/v,  $c = 3 \text{ mmol L}^{-1}$ ) solvent. Image (b) SEM and (d) TEM showing nanorod like architectures in a THF–water (1 : 1 v/v,  $c = 5 \text{ mmol L}^{-1}$ ) solvent.



**Fig. 4** Schematic representation for the formation of spheres and salt-promoted disruption followed by microscopic transformations to aligned nanofibers by peptide P1 in methanol : water. (a) Fluorescence microscopy image of rhodamine B dye ( $0.0312 \text{ mmol L}^{-1}$  in methanol : water 1 : 1) entrapped sphere like structures of P1 in methanol : water (1 : 1 v/v,  $c = 3.0 \text{ mmol L}^{-1}$ ). Images (b) SEM, (d) TEM and (c) SEM, (e) TEM illustrate the disruption of spheres with  $\text{CaCl}_2$  solution ( $c = 3.0 \text{ mmol L}^{-1}$  in methanol : water (1 : 1 v/v)) and  $\text{NaCl}$  solution ( $c = 3.0 \text{ mmol L}^{-1}$  in methanol : water (1 : 1 v/v)) resulting in microscopic transformation to aligned nanofibers respectively under ambient conditions.

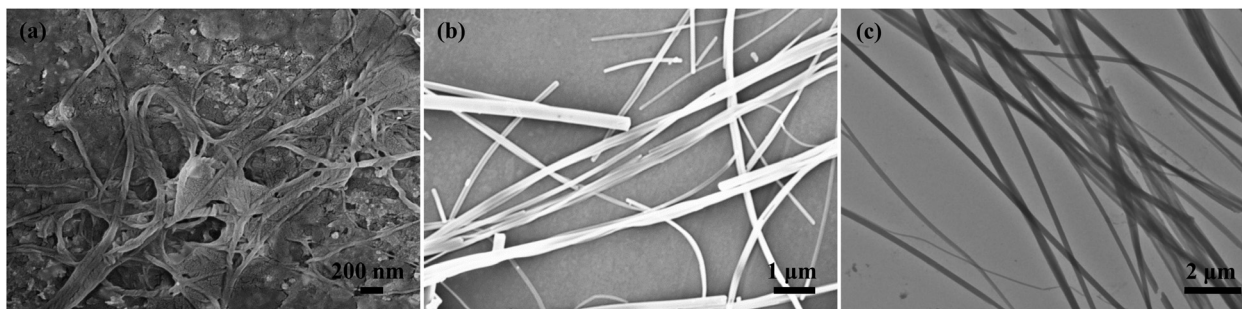


**Fig. 5** Electron microscopy analysis shows twisted nanofibers and nanorod like morphology of peptides P2 and P3. Image (a) SEM illustrates the formation of twisted nanofibers, which are organized for P2 in methanol : water (1 : 1 v/v,  $c = 3.0 \text{ mmol L}^{-1}$ ). Images (b) SEM and (c) TEM showing the formation of a nanorod like structural design, which are organized from P3 in THF : water (1 : 1 v/v,  $c = 3.0 \text{ mmol L}^{-1}$ ).

mental conditions employed for the microscopy study of P1 in aqueous methanol. The average width of the nanorod observed by SEM analysis is 500 nm, whereas in TEM images these nanorods have a width ranging from 150 nm to 700 nm.

Furthermore, the spherical morphology was also studied by entrapment of a fluorescent dye rhodamine B and alkali metal salt-prompted disruption. Fig. 4a clearly demonstrates the encapsulation of rhodamine B dye under ambient conditions. The mixed aqueous methanolic (1 : 1) solution of P1 with rhodamine B dye<sup>29</sup> was studied by a fluorescence microscopy experiment. We examined disruption of these spherical aggregates by a salt-induced disruption study using  $\text{CaCl}_2$  and NaCl solutions. A few examples have been reported in the literature which describe the interaction of cations to the aromatic residues of aromatic amino acids in peptides, which result in morphological changes.<sup>30</sup> Interestingly, in our experiment, we observe the cation-responsive morphological transformations of peptide P1 (Fig. 4 and S7†). Morphological transformation of peptides by external stimuli has been also demonstrated by several groups.<sup>31,32</sup> In our study, spherical aggregates were ruptured simply by adding  $\text{CaCl}_2$  and NaCl solutions ( $3.0 \text{ mmol L}^{-1}$ ) to peptide P1 ( $3.0 \text{ mmol L}^{-1}$ ) in a methanol–water (1 : 1) solution. SEM and TEM studies revealed that the rapture of spheres prompted the formation of a bunch of aligned mineralized nanofibrillar architectures (Fig. 4b–e). Biologically important metal ions have an essential role to stabilize the higher-order self-assembled structures made up of biopolymers, by which many important biochemical tasks can be executed. The mineralization and interaction of biocompatible metal ions on the surface of peptide-assemblages have been demonstrated and could also show promising applications in biotechnology and material sciences.<sup>33</sup> Stupp *et al.* recently illustrated the alignment of peptide amphiphilic nanofibers, which can be driven by a thermal pathway.<sup>34</sup> Tovar *et al.* also demonstrated the formation of aligned nanofibers of  $\pi$ -conjugated polydiacetylene-peptide amphiphiles by an extrusion technique.<sup>35</sup> Our results depict the accumulations of aligned mineralized nanofibers from spheres resulting from disruption of alkali metal salt under ambient conditions. Depending on the nature of cations ( $\text{Ca}^{2+}$  or  $\text{Na}^+$ ), spheres transform into size variable nanofibers. SEM results of the  $\text{CaCl}_2$  disruption

study (Fig. 4b) demonstrate the generation of elongated fibers. The average width of the fibers is found to be 660 nm and the length of the fibers is several micrometers. Fig. 4c shows SEM results of the NaCl disruption study, which illustrates the accumulation of a fibrous-architecture with an average width of 500 nm with several micrometers in length. In addition, TEM images (Fig. 4d and e) also support the transformation of spheres to fibers. The average width of nanofibers is 825 nm and 160 nm which result from the  $\text{CaCl}_2$  and NaCl disruption study respectively. Mineralization of peptide nanofibers by metal ions was supported by EDX analysis (Fig. S8†).<sup>36</sup>

Fig. 5 depicts morphological features of peptide P2 in methanol–water (1 : 1) and peptide P3 in THF–water (1 : 1) solvents. The SEM image of peptide P2 shows helical nanofibrillar structures having an average diameter of 40 nm. These helical nanofibers twisted again and formed a more wide twisted nanofibrillar architecture (Fig. S9†). It is well known that supramolecular chirality of nanostructures is gained from molecular chirality and self-assembly of chiral building blocks.<sup>37</sup> SEM observation of peptide P3 in the THF–water (Fig. 5b) solvent exhibits elongated and cross-linked nanofibrillar structures. The average width of these nanostructures is found to be 200 nm with several micrometers in length. Transmission electron microscopy images of peptide P3 in THF–water (Fig. 5c) demonstrate the presence of cross-linked nanofibrillar aggregation which is similar to that of the SEM analysis of peptide P3. TEM results are in accordance to that of the SEM results with an average width of 200 nm and several micrometers in length of peptide P3 nanostructures.

Thus, from all the morphological results, it is noted that the hydrophobicity (contribution of the side chain) of the amino acids and the solvent polarity play an important role in morphological diversity. The presence of external stimuli such as metal ions is also responsible for molecular packing at the supramolecular level and the formation of tunable nanostructures.<sup>14a,38</sup>

#### Conformational analysis of peptides in solid state

The results obtained by 2D NMR studies as reported above clearly revealed the double-turn conformation of peptides in  $\text{CDCl}_3$ . However, we were enthused to probe the conformational analysis and supramolecular structure of these synthesized

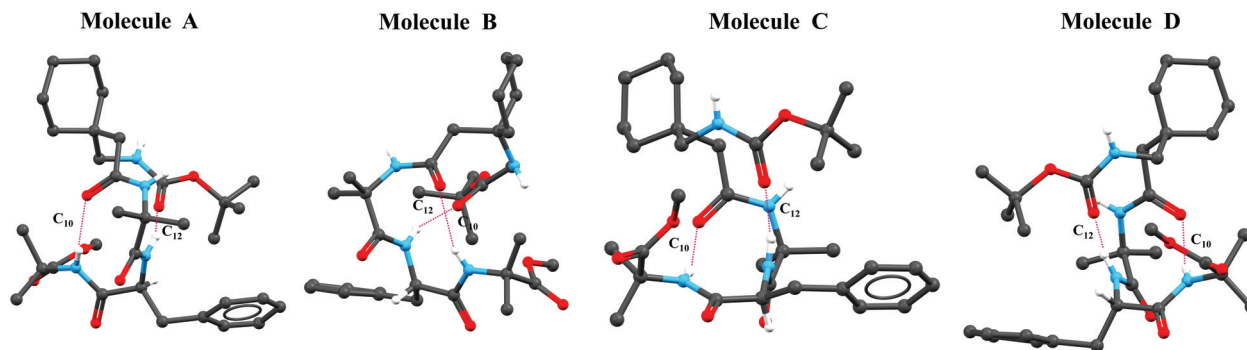


Fig. 6 Crystal structure of P1 displaying a  $C_{12}/C_{10}$  hydrogen-bonded double turn conformation and four molecules observed in the asymmetric unit, named as molecule A, molecule B, molecule C and molecule D. Hydrogen atoms are removed for clarity. Hydrogen-bonds are shown as dotted lines.

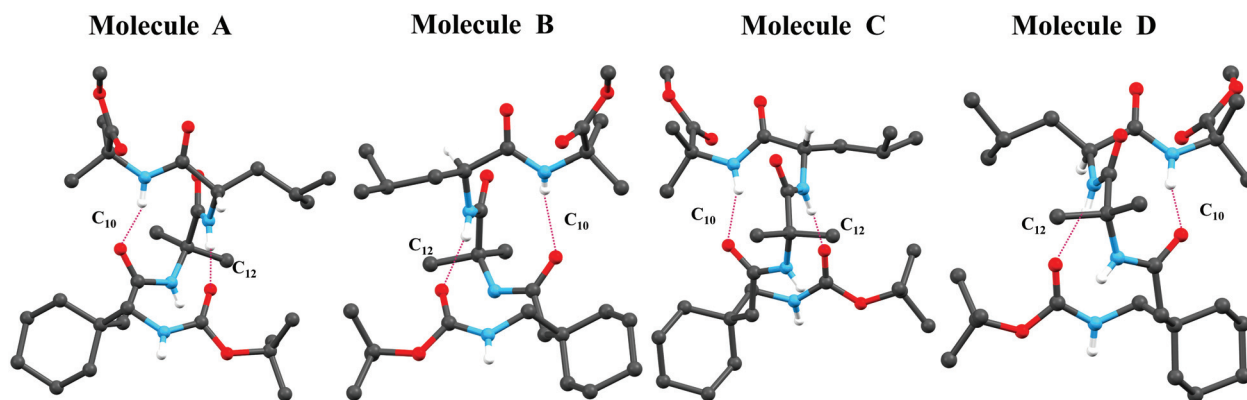


Fig. 7 Crystal structure of P2 displaying a  $C_{12}/C_{10}$  hydrogen-bonded double turn conformation and four molecules observed in the asymmetric unit, named as molecule A, molecule B, molecule C and molecule D. Hydrogen atoms are removed for clarity. Hydrogen-bonds are shown as dotted lines.

peptides in a solid state. In this regard, we attempted to grow crystals of P1–P3 in various combinations of solvents. Diffraction possible good quality single crystals were obtained from the slow evaporation of P1 in DMSO and isopropanol solutions and P2 and P3 crystals were grown from methanol/water mixtures. Peptides P1 and P2 were crystallized with four peptide molecules named molecule A, molecule B, molecule C and molecule D in the asymmetric unit, whereas peptide P3 was crystallized with two peptide molecules named molecule A and molecule B in the asymmetric unit (Table S2<sup>†</sup>).

Fig. 6–8 depict atomic resolution conformations of peptides P1, P2 and P3. In spite of being different at the third position in all three peptides (P1–P3) a  $C_{12}/C_{10}$  double turn hydrogen-bonded folded fashion was found in all three cases. Solid-state structures of P1, P2 and P3 reveal 12-membered unusual  $1 \leftarrow 4$  type hydrogen-bonding interactions between  $C=O$  (Boc,  $i$ )  $\cdots$   $H-N$  ( $3, i+3$ ). The  $C_{12}$  H-bond is located between (Boc)  $C=O \cdots H-N$  (Xaa = Phe for P1, Xaa = Leu for P2 and Xaa = Tyr for P3). The *gem* dialkyl substitution at  $C^\beta$  position of Gpn restricts the torsion angles of  $C^\gamma-C^\beta$  ( $\theta_1$ ),  $C^\beta-C^\alpha$  ( $\theta_2$ ) to about  $\pm 60^\circ$  (Table S3<sup>†</sup>), which facilitate the formation of the  $C_{12}$  hydrogen-bonded turn.

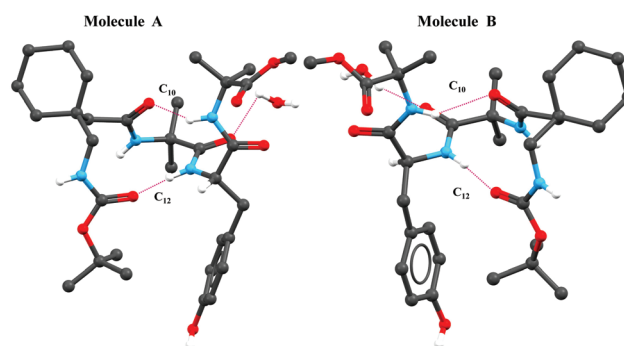
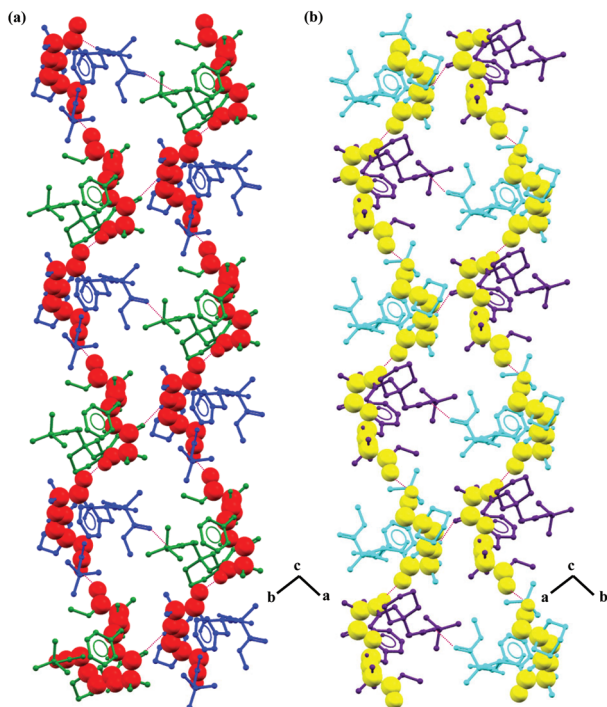


Fig. 8 Crystal structure of P3 displaying a  $C_{12}/C_{10}$  hydrogen-bonded double turn conformation and two molecules observed in the asymmetric unit, named as molecule A (along with one water molecule) and molecule B (along with one water molecule). Hydrogen atoms are removed for clarity. Hydrogen-bonds are shown as dotted lines.

In addition to the  $C_{12}$  H-bonded turn, there is one more 10-membered hydrogen-bonded  $\beta$ -turn, observed in each molecule of P1, P2 and P3. This additional  $C_{10}$  H-bonded turn is formed adjacent to the  $C_{12}$  H-bonded turn due to the inter-



**Fig. 9** The packing diagram and supramolecular helical view of peptide P1 in the crystal structure. (a) Molecule A (green colour) and molecule B (dark blue colour) are aligned and stacked with one on top of the other to form supramolecular helices. (b) Supramolecular helices formed by molecule C (purple colour) and molecule D (sky blue colour). Hydrogen atoms are removed for clarity. Hydrogen-bonds are shown as dotted lines.

action between (Gpn(1))C=O...H-N(Aib(4)) which is located over the Aib(2)-Xaa(3)-Aib(4)  $\alpha\alpha\alpha$  segment. Torsion angles of peptides P1, P2 and P3 in crystal structures are summarized in Table S3.† Four individual molecules of P1 and P2 and two individual molecules of P3 in the asymmetric unit are folded into a  $C_{12}/C_{10}$  hydrogen-bonded double turn conformation. These 12-atom hydrogen-bonded conformations can be viewed as expanded 10-membered hydrogen-bonded  $C_{10}$  turn which is found in  $\alpha$ -polypeptides.<sup>15</sup>  $C_{10}$  hydrogen-bonded units in P1–P3 form  $\beta$ -turn conformations. The segment Aib(2)-Phe(3)-Aib(4) of P1 forms type I'  $\beta$ -turn, type I  $\beta$ -turn, type I  $\beta$ -turn and type I'  $\beta$ -turn in molecules A, B, C and D respectively. The segment Aib(2)-Leu(3)-Aib(4) of P2 forms a type I  $\beta$ -turn, type III'  $\beta$ -turn, type I  $\beta$ -turn and type III'  $\beta$ -turn in molecules A, B, C and D respectively. Moreover, Aib(2)-Tyr(3)-Aib(4) forms type III'  $\beta$ -turn and type I  $\beta$ -turn in molecule A and molecule B respectively in P3.<sup>6f</sup> Type I/I' and Type III/III' turns are closely associated with each other.<sup>6f,15</sup>

### Molecular packing in supramolecular level

Short synthetic peptides can be self-assembled to form supramolecular motifs like supramolecular helices and double helices.<sup>3,4a,39,40</sup> Peptides are assembled at the supramolecular level to give interesting structural motifs in crystals and solution phase. Here, the reported three peptides P1, P2 and P3 give double turn conformations in crystal structures and further self-assemble to form diverse supramolecular helical architectures (Fig. 9–11).

In the crystal structure of P1, the independent peptide molecules are self-assembled through intermolecular hydro-

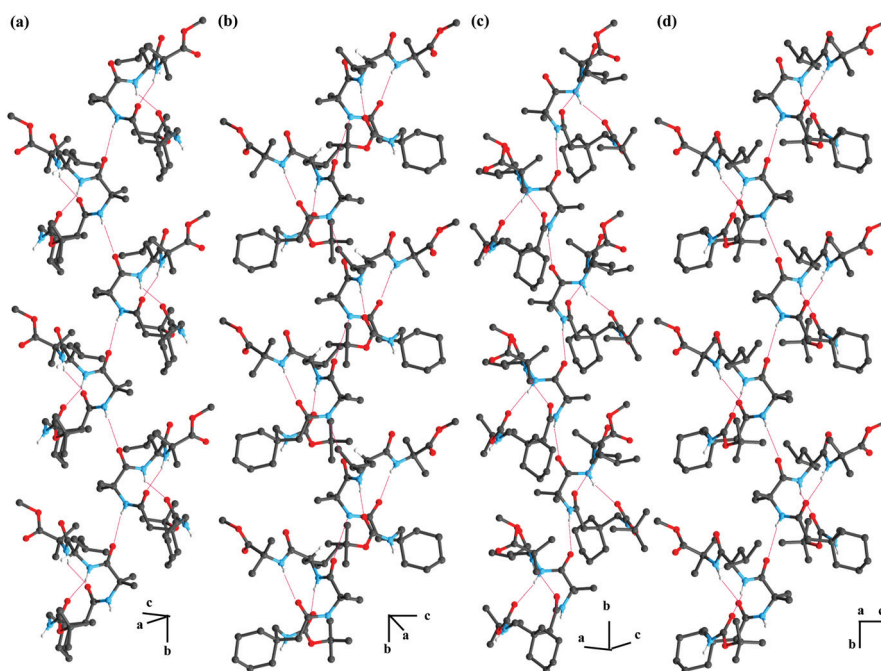


**Fig. 10** Supramolecular helical architecture of peptide P2 in solid state. Supramolecular helical architecture formed from (a) molecule A, (b) molecule B, (c) molecule C and (d) molecule D. Hydrogen atoms are removed for clarity. Hydrogen-bonds are shown as dotted lines.

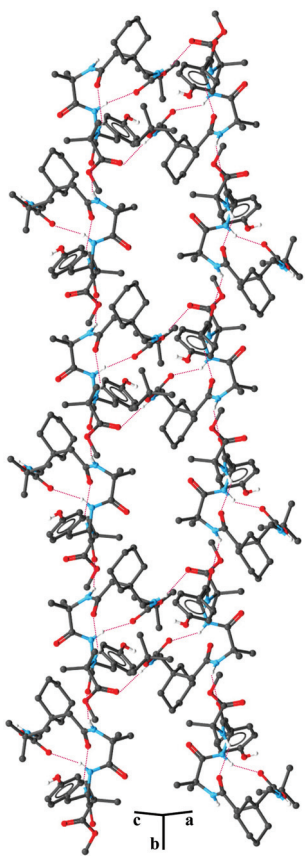


**Fig. 11** A higher order packing diagram of peptide P3 showing formation of supramolecular helices along the crystallographic *b* axis. Supramolecular helices individually formed by the linear-association of molecules A and B by stacking with one on top of the other. These supramolecular helices are self-associated to form higher order architecture. Hydrogen atoms are removed for clarity. Hydrogen-bonds are shown as dotted lines.

gen-bonds and various non-covalent interactions to form highly ordered supramolecular helical structures (Fig. 9). Molecules A and B, and molecules C and D in the asymmetric unit are co-ordinated *via* two different intermolecular hydrogen-bonds along the *b*- and *a*-axis. These inter-molecular H-bonds originate between Aib(4) C=O of molecule A and H-N Gpn(1) of molecule B, Aib(2) C=O of molecule D and H-N Aib(2) of molecule C. In higher order self-assembly, molecules A and B are aligned and stacked to form supramolecular helical architectures using inter-molecular hydrogen-bonds. Similarly, molecules C and D are aligned and stacked to form a supramolecular helix using repeated inter-molecular H-bonds which originate between Aib(4) C=O of molecule C and H-N Gpn(1) of molecule D, Aib(2) C=O of molecule D and H-N Aib(2) of molecule C. The supramolecular helical assemblies formed by molecules A, B and molecules C, D are interconnected *via* inter-molecular H-bonds. The peptide subunits in each supramolecular helical structure preserve proper registry and subsequently these supramolecular helical structures are self-associated to form higher ordered structures by inter-molecular hydrogen-bonds and other non-covalent interactions.

Close investigation of the crystal structure of P2 reveals that double bended peptide subunits are organized to form supramolecular helices through several intermolecular hydrogen-bonds (Fig. 10). Molecules A, B and C, D are co-ordinated in a head to tail fashion by two types of intermolecular H-bonds in the asymmetric unit along the *c*-axis (Table 2). These H-bonds are Aib(4) C=O of molecule A/B/C/D with H-N Gpn(1) of molecule B/A/D/C. In the higher order self-assembly, molecule A is coordinated with the other adjacent molecule A using repeated inter-molecular hydrogen bonds to form a supramolecular helix along the *b*-axis. Similarly molecule B, C and D individually co-ordinate to form a supramolecular helix by inter-molecular H-bonds.

A doubly hydrated crystal structure is revealed for peptide P3, which was grown in a methanol-water solution. Two water molecules are crystallized in the asymmetric unit along with two peptide molecules namely molecules A and B. The individual molecules A and B are connected in a head to tail fashion with two inter-molecular hydrogen-bonds. These H-bonds are Aib(4) C=O of molecule A/B with H-N Gpn(1) of molecule B/A. Simultaneously molecules A and B interact with water molecules using Aib(2)C=O and H-O (water) co-ordinates. The solid state structure of P3 reveals that double turn structures of peptide subunits are orderly organized by several inter-molecular hydrogen-bonds to form highly ordered supramolecular helical motifs along the crystallographic *b* axis (Fig. 11). Previous reports have shown that water molecules play an important role to form and stabilize supramolecular helical structures in short peptides.<sup>39b</sup> The crystal structure of P3 shows interesting supramolecular assemblies (Fig. 11 and S10†), which are generated by the regular alignment of each peptide subunit and water molecules through various potential non-covalent interactions. Fig. 11 clearly explains that molecules A or B individually stack one on top of the other *via* inter-molecular hydrogen-bonds along the crystallographic *b* axis. These supramolecular helical structures are generated by the linear-association of molecules A and B through Tyr(3) C=O...H-N Aib(2) intermolecular hydrogen-bond interactions along the crystallographic *b* axis. Phenolic O-H functionality of Tyr(3) in P3 is inter-molecularly hydrogen-bonded with water molecules (Table 2). The side chain phenolic O-H functionality of Tyr(3) in P3 plays an important role in the formation of supramolecular arrays *via* interactions between the peptide molecules and water molecules. The individual supramolecular strands (helical strand formed by molecules A and B) are further associated by intervening bridged water molecules through various H-bond interactions to form higher order supramolecular assemblies. From this supramolecular investigation, we noticed that peptides P1, P2 and P3 self-assemble to form diverse supramolecular architectures using various non-covalent interactions. Molecules A, B or C, D of peptide P1 collectively self-assemble to form a supramolecular helix along the *b*- and *a*-axis. Whereas, peptide P2 subunits (molecules A, B, C and D) are individually interconnected to form a supramolecular helix along the *b*-axis. Interestingly, peptide P3 forms a highly ordered supramolecular architecture

Table 2 Hydrogen bond parameters of peptide P1, P2 and P3

Peptide	Type of hydrogen-bond	D–H...A	H...A (Å)	D...A (Å)	∠D–H...A (°)
<b>P1</b>					
Molecule A	Intramolecular	N014–H014...O001	2.02	2.74	142.0
		N1A–H1A...O00M	2.20	3.02	160.5
	Intermolecular	N1C–H1C...O00B	2.26	2.88	128.7
		N00X–H00X...O00Y	2.07	2.92	169.0
Molecule B	Intramolecular	N1W–H1W...O016	2.07	2.88	158.2
		N1E–H1E...O005	2.30	3.11	156.6
	Intermolecular	N2K–H02V...O00H	2.15	2.86	139.5
		N011–H011...O008	2.06	2.91	172.3
Molecule C	Intramolecular	N1T–H1T...O01L	2.02	2.83	156.0
		N2P–H2P...O006	2.29	3.10	156.4
	Intermolecular	N1J–H1J...O00S	2.30	2.94	131.5
		N2T–H2T...O009	2.10	2.95	170.1
Molecule D	Intramolecular	N1Q–H1Q...O003	2.00	2.72	141.2
		N2Z–H2Z...O00K	2.24	3.03	152.7
	Intermolecular	N2J–H2J...O01A	2.41	2.97	123.0
		N2O–H2O...O00L	2.07	2.92	168.3
<b>P2</b>					
Molecule A	Intramolecular	N00N–H00N...O00S	1.98	2.75	149.0
		N00U–H00U...O008	2.15	2.93	150.0
	Intermolecular	N1A–H1AA...O00R	1.95	2.81	178.5
		N012–H012...O00O	2.06	2.91	172.0
Molecule B	Intramolecular	N00K–H00K...O00C	2.10	2.94	166.0
		N014–H5...O007	2.42	3.04	173.4
	Intermolecular	N012–H012...O00O	2.06	2.91	172.0
		N1A–H1AA...O00R	1.95	2.81	178.5
Molecule C	Intramolecular	N00P–H00P...O005	2.07	2.90	160.0
		N00Z–H00Z...O001	2.19	2.97	152.3
	Intermolecular	N013–H013...O01M	2.04	2.88	166.0
		N1U–H1U...O004	2.00	2.84	166.0
Molecule D	Intramolecular	N00X–H00X...O010	1.99	2.80	160.0
		N00Y–H2...O00E	2.09	3.04	162.6
	Intermolecular	N1U–H1U...O004	2.00	2.84	166.0
		N013–H013...O01M	2.04	2.88	166.0
<b>P3</b>					
Molecule A	Intramolecular	N3–H3...O6	1.99	2.73	144.5
		N4–H4...O5	2.17	2.88	139.1
		N1–H1...O13	2.06	2.92	176.0
	Intermolecular	N2–H2...O3	2.23	2.97	143.6
		O17–H17...O20W	2.00	2.73	146.5
		O20W–H501W...O4	2.30	2.75	109.6
Molecule B	Intramolecular	N7–H7...O9	2.15	2.94	160.1
		N8–H8...O10	2.29	3.03	144.2
		N5–H5...O2	2.23	3.05	158.6
	Intermolecular	N6–H6...O12	2.18	2.97	152.3
		O18–H18...O50W	2.01	2.77	155.7
		O50W–H60W...O11	1.91	2.78	161.2

where phenolic –OH side chain functionality and bridged water molecules play an important role to stabilize such well-organized and packed supramolecular helices. The side chain orientations of the third residue in peptides P1–P3 and non-covalent interactions among side chains and neighbor molecules at the supramolecular level are responsible for diverse supramolecular architectures.

## Conclusion

In summary, we have synthesized and demonstrated the structural propensities of Gpn containing hybrid peptides P1–P3 by 2D-NMR spectroscopy and single crystal X-ray diffraction studies. The 2D NMR analysis reveals that double turn conformations are being adopted *via* C<sub>12</sub> and C<sub>10</sub> intramolecular hydrogen-bonds. The crystal structure also reveals a double turn folded conformation adopted by hybrid peptides P1–P3, irrespective of their third amino acid residue. The conformationally rigid unnatural amino acids ( $\alpha$ -aminoisobutyric acid and gabapentin) induce the reported peptide backbones to adopt into a folded double turn C<sub>12</sub>/C<sub>10</sub> hydrogen-bonded conformation. The reported peptides P1–P3 display diversity in supramolecular and morphological propensities in solid as well as solution states, which is attributed to the backbone side chain variation at the third position of the peptide sequence. The circular dichroism studies show distinct CD patterns for peptides P1–P3 in an aqueous methanol medium which can be attributed to the third residue side-chain effect. Both scanning and transmission electron microscopy obser-

ations are being adopted *via* C<sub>12</sub> and C<sub>10</sub> intramolecular hydrogen-bonds. The crystal structure also reveals a double turn folded conformation adopted by hybrid peptides P1–P3, irrespective of their third amino acid residue. The conformationally rigid unnatural amino acids ( $\alpha$ -aminoisobutyric acid and gabapentin) induce the reported peptide backbones to adopt into a folded double turn C<sub>12</sub>/C<sub>10</sub> hydrogen-bonded conformation. The reported peptides P1–P3 display diversity in supramolecular and morphological propensities in solid as well as solution states, which is attributed to the backbone side chain variation at the third position of the peptide sequence. The circular dichroism studies show distinct CD patterns for peptides P1–P3 in an aqueous methanol medium which can be attributed to the third residue side-chain effect. Both scanning and transmission electron microscopy obser-

vations demonstrate solvent dependent self-assembled morphological features as well as morphological transformations by biocompatible metal ions such as  $\text{Ca}^{2+}$  and  $\text{Na}^+$  under ambient conditions. The designed hybrid peptides constructed from proteolytically stable and conformationally rigid Gpn and  $\alpha$ -aminoisobutyric acid and their nanostructural features may find useful applications in nanoscience and nanotechnology.

## Experimental section

### X-ray crystallography

Crystallographic data for all three compounds were collected on a Rigaku FRX microfocussing rotating anode (3 kW) at the copper  $\text{K}\alpha$  edge equipped with a Dectris Pilatus 200 K hybrid detector. Structures were solved using SHELXD (structure P1) and SHELXT (structures P2 and P3). All data were processed with the CrystalClear suite version 2.1b25. The structures were refined using SHELXL 2014 version.<sup>41</sup> Full-matrix least-squares refinement was performed on  $F^2$  for all unique reflections, minimizing  $w(F_o^2 - F_c^2)^2$ , with anisotropic displacement parameters for non-hydrogen atoms. All H atoms found in difference electron-density maps were refined freely, all the others were treated as riding on their parent C or N atoms. Data statistics are reported in the Table S1† and cif files. Although the structure of peptide P1 can be solved in the monoclinic  $P2_1$  space group with two molecules in the ASU, this structure was finally refined in the triclinic  $P1$  space group with four molecules in the ASU leading to more accurate thermal motion parameters and better overall refinement statistics. Crystallographic data of P1, P2 and P3 have been deposited with the CCDC: 1054010 (P1), 1463837 (P2) and 1054011 (P3).

### Circular dichroism (CD) spectroscopy

Circular dichroism (CD) spectra were obtained on a Jasco J-815 spectropolarimeter. Spectra were measured between 300 to 190 nm with 0.1 nm data pitch, 1 nm bandwidth, 20 nm  $\text{min}^{-1}$  scanning speed and a response time of 1 s. A quartz cell (Starna Scientific Ltd Hainault, UK) with a path length of 1 mm was used. Samples were prepared by dissolving the peptides in methanol and diluting with water (Milli-Q) to get a final concentration as stated in the CD spectra. Experimental data were acquired thrice and the average data is shown.

### NMR spectroscopy

All NMR spectra of peptides were recorded on a Bruker AV 400 MHz spectrometer at 298 K. The concentrations were in the range of 1–10  $\text{mmol L}^{-1}$  in  $\text{CDCl}_3$  and  $\text{DMSO-}d_6$  for  $^1\text{H}$  and  $^{13}\text{C}$ -NMR. The concentration for DMSO titration studies was 20  $\text{mmol L}^{-1}$  and for 2D-NMR experiments was 30  $\text{mmol L}^{-1}$ . Chemical shifts were expressed in parts per million (ppm,  $\delta$ ) relative to residual solvent protons as internal standards ( $\text{CHCl}_3$ :  $\delta$  7.26,  $\text{DMSO}$ : 2.50 for  $^1\text{H}$ ,  $\text{CHCl}_3$ :  $\delta$  77.00,  $\text{DMSO}$ : 39.50 for  $^{13}\text{C}$ ).  $^1\text{H}$ -NMR multiplicities were designated as singlet (s), doublet (d), triplet (t), quartet (q) multiplet (m) and broad singlet (bs).  $^1\text{H}$  NMR spectra assignments of three pep-

tides were achieved by using a combination of 2D COSY and ROESY experiments. All the ROESY NMR experiments were recorded at 298 K with a mixing time of 200 ms.

### Microscopy study

Peptide solutions were prepared by mixing of 1.8 mg of P1 and 1.7 mg of P2 respectively in 0.5 mL of methanol in individual vials. Peptides were completely dissolved by shaking. Distilled water (Milli-Q water) was added to 0.5 mL of peptide solutions to set the final peptide concentration to 3  $\text{mmol L}^{-1}$  and allowed to stand at room temperature for 30 minutes for SEM analysis. Peptide solutions were also prepared by mixing 1.8 mg of P1 and 1.85 mg of P3 respectively in 0.5 mL of tetrahydrofuran. Peptides were completely dissolved by shaking. The peptide solutions were added to 0.5 mL of pre-cooled vigorously stirring distilled water (Milli-Q water) in another three sets of vials. The final concentration of peptide solutions was set to 3  $\text{mmol L}^{-1}$  and allowed to stand at room temperature for 30 minutes for microscopy analysis.

$\text{CaCl}_2$  and  $\text{NaCl}$  solutions (6  $\text{mmol L}^{-1}$ ) were prepared in methanol:water (1:1 v/v). 0.5 mL of the prepared salt solutions was added separately to the freshly prepared 0.5 mL of peptide P1 (6  $\text{mmol L}^{-1}$ ) in methanol:water (1:1 v/v). Thus, the final concentrations of salt-peptide mixed solutions were set to 3  $\text{mmol L}^{-1}$  and allowed to stand at room temperature for 30 minutes. 100  $\mu\text{L}$  of prepared peptide solutions was drop-casted on clean and dried glass slides and they were allowed to dry in air at room temperature followed by microscopy measurements. The self-assembled peptide samples were drop-casted on a glass slide, coated with gold and measured SEM was performed on a Carl Zeiss Microscope (model-Supra 55). Transmission electron microscopy images were taken using a PHILIPS electron microscope (Model: CM 200), operated at an accelerating voltage of 200 kV. The self-assembled peptide samples were dried on carbon-coated copper grids (300 mesh) by slow evaporation in air and then allowed to dry separately in vacuum at room temperature.

### Fluorescence microscopy study

Peptide P1 was dissolved in 1 mL of rhodamine B (0.0312  $\text{mmol L}^{-1}$ ) in a methanol-water (1:1 v/v) solution to make a final concentration of 3  $\text{mmol L}^{-1}$ . The solution was kept at room temperature for 3 h. From this prepared solution, 20  $\mu\text{L}$  was drop-casted on a clean and dried cover slip. The sample was allowed to dry in air at room temperature, followed by fluorescence microscopy measurements. Fluorescence microscopy experiments were performed on a home-built epifluorescence microscopy set-up. An air-cooled argon ion laser (Melles Griot, model 400-A03) with an excitation wavelength of 488 nm was used to excite the spherical structure sample placed on an inverted microscope (Nikon, model Eclipse Ti-U). The laser beam was expanded and subsequently focused on the back-focal plane of an oil immersion objective (100  $\times$  1.49 NA Nikon) to illuminate a 60  $\times$  60  $\mu\text{m}^2$  area of the sample. The PL from the sample was recorded by a B2A filter cube (Nikon) with a 505 nm dichroic mirror and a 520 nm long-pass

filter and finally imaged with a back-illuminated EMCCD camera (Andor, model iXon X3 897) at an exposure time of 300 ms. The images were analyzed with ImageJ (Version 1.46r) NIH.

### Polarimeter measurement

Specific rotations of reported peptides were measured on an Autopol® V automatic polarimeter (Rudolph research analytical). The cell with length = 100 mm and capacity = 2 mL was used for this study at 20 °C.

### FT-IR spectroscopy

FT-IR spectroscopy of all reported peptides was performed using a Bruker (Tensor-27) FT-IR spectrophotometer. The KBr pellet technique was used and scanned between 500 cm<sup>-1</sup> to 4000 cm<sup>-1</sup> over 64 scans at a resolution of 4 cm<sup>-1</sup> and at an interval of 1 cm<sup>-1</sup>.

### Mass spectrometry

Mass spectra were recorded on a Bruker micrOTOF-Q II by positive-mode electrospray ionization.

## Acknowledgements

AKD sincerely acknowledges Department of Science & Technology (Nanomission) Project no. SR/NM/NS-1458/2014, New Delhi, India for financial support. MK is indebted to CSIR, New Delhi, India for his fellowship for this work. D. B. R. is thankful to IIT Indore, India, for a postdoctoral fellowship. The sophisticated instrumentation centre (SIC), IIT Indore is acknowledged for providing access to the instrumentation. We thank Dr T. K. Sarma, IIT Indore, India for providing access to DLS experiments. We thank SAIF, IIT Bombay, India for assistance with the TEM facility.

## Notes and references

- (a) T. Aida, E. W. Meijer and S. I. Stupp, *Science*, 2012, **335**, 813–817; (b) M. Zelzer and R. V. Ulijn, *Chem. Soc. Rev.*, 2010, **39**, 3351–3357; (c) Z. N. Mahmoud, S. B. Gunnoo, A. R. Thomson, J. M. Fletcher and D. N. Woolfson, *Biomaterials*, 2011, **32**, 3712–3720; (d) T. Hiroshi and M. Hisakazu, *Mol. BioSyst.*, 2013, **9**, 609–617.
- (a) P. Gonzalez-Tello, F. Carnacho, E. Jurado, M. P. Paez and E. M. Guadix, *Biotechnol. Bioeng.*, 1994, **44**, 529–532; (b) M. C. Marquez and M. A. Vazquez, *Process Biochem.*, 1999, **35**, 111–117.
- Foldamers: Structure, Properties, and Applications*, ed. S. Hecht and I. Huc, Wiley-VCH, Verlag GmbH & Co., Weinheim, Germany, 2007.
- (a) G. Guichard and I. Huc, *Chem. Commun.*, 2011, **47**, 5933–5941; (b) C. M. Goodman, S. Choi, S. Shandler and W. F. DeGrado, *Nat. Chem. Biol.*, 2007, **3**, 252–262.
- (a) D. Seebach and J. Gardiner, *Acc. Chem. Res.*, 2008, **41**, 1366–1375; (b) T. A. Martinek and F. Fulop, *Chem. Soc. Rev.*, 2012, **41**, 687–702; (c) P. Claudon, A. Violette, K. Lamour, M. Decossas, S. Fournel, B. Heurtault, J. Godet, Y. Mely, B. J. Gregoire, M. C. A. Petit, J. P. Briand, G. Duportail, H. Monteil and G. Guichard, *Angew. Chem., Int. Ed.*, 2010, **49**, 333–336.
- (a) D. Seebach and J. L. Matthews, *Chem. Commun.*, 1997, 2015–2022; (b) D. Seebach, D. F. Hook and A. Glattli, *Biopolymers*, 2006, **84**, 23–37; (c) S. H. Gellman, *Acc. Chem. Res.*, 1998, **31**, 173–180; (d) R. P. Cheng, S. H. Gellman and W. F. DeGrado, *Chem. Rev.*, 2001, **101**, 3219–3232; (e) W. S. Horne and S. H. Gellman, *Acc. Chem. Res.*, 2008, **41**, 1399–1408; (f) G. D. Rose and L. M. Gierasch, *Adv. Protein Chem.*, 1985, **37**, 1–109; (g) P. G. Vasudev, S. Chatterjee, N. Shamala and P. Balaram, *Chem. Rev.*, 2011, **111**, 657–687.
- (a) G. V. M. Sharma, V. B. Jadhav, K. V. S. Ramakrishna, P. Jayaprakash, K. Narsimulu, V. Subash and A. C. Kunwar, *J. Am. Chem. Soc.*, 2006, **128**, 14657–14668; (b) G. V. M. Sharma, N. Chandramouli, M. Choudhary, P. Nagendar, K. V. S. Ramakrishna, A. C. Kunwar, P. Schramm and H.-J. Hofmann, *J. Am. Chem. Soc.*, 2009, **131**, 17335–17344; (c) L. K. A. Pilsl and O. Reiser, *Amino Acids*, 2011, **41**, 709–718.
- (a) P. G. Vasudev, N. Shamala, K. Ananda and P. Balaram, *Angew. Chem., Int. Ed.*, 2005, **44**, 4972–4975; (b) I. L. Karle and P. Balaram, *Biochemistry*, 1990, **29**, 6747–6756.
- (a) V. V. E. Ramesh, G. Priya, A. S. Kotmale, R. G. Gonnade, P. R. Rajamohan and G. J. Sanjayan, *Chem. Commun.*, 2012, **48**, 11205–11207; (b) S. S. Kale, S. M. Kunjir, R. L. Gawade, V. G. Puranik, P. R. Rajamohan and G. J. Sanjayan, *Chem. Commun.*, 2014, **50**, 2886–2888.
- (a) M. G. Woll, J. R. Lai, I. A. Guzei, S. J. C. Taylor, M. E. B. Smith and S. H. Gellman, *J. Am. Chem. Soc.*, 2001, **123**, 11077–11078; (b) M. Hagihara, N. J. Anthony, T. J. Stout, J. Clardy and S. L. Schreiber, *J. Am. Chem. Soc.*, 1992, **114**, 6568–6570; (c) M. K. N. Qureshi and M. D. Smith, *Chem. Commun.*, 2006, 5006–5008; (d) J. Farrera-Sinfreu, L. Zaccaro, D. Vidal, X. Salvatella, E. Giralt, M. Pons, F. Albericio and M. Royo, *J. Am. Chem. Soc.*, 2004, **126**, 6048–6057; (e) A. Kothari, M. K. N. Qureshi, E. M. Beck and M. D. Smith, *Chem. Commun.*, 2007, **47**, 2814–2816.
- (a) I. Huc, *Eur. J. Org. Chem.*, 2004, 17–29; (b) N. Delsuc, S. Massip, J.-M. Leger, B. Kauffmann and I. Huc, *J. Am. Chem. Soc.*, 2011, **133**, 3165–3172; (c) S. K. Maity, S. Maity, P. Jana and D. Haldar, *Chem. Commun.*, 2012, **48**, 711–713.
- L. Mathieu, B. Legrand, C. Deng, L. Vezenkov, E. Wenger, C. Didierjean, M. Amblard, M.-C. Averlant-Petit, N. Masurier, V. Lisowski, J. Martinez and L. T. Maillard, *Angew. Chem., Int. Ed.*, 2013, **52**, 6006–6010.
- (a) Y. Hamuro, S. J. Geib and A. D. Hamilton, *J. Am. Chem. Soc.*, 1996, **118**, 7529–7541; (b) B. Gong, Y. Yan, H. Zeng, E. S. Jankunn, Y. W. Kim, J. Zhu and H. Ickes, *J. Am. Chem. Soc.*, 1999, **121**, 5607–5608.

- 14 (a) P. Koley and A. Pramanik, *Adv. Funct. Mater.*, 2011, **21**, 4126–4136; (b) P. Koley and A. Pramanik, *Soft Matter*, 2012, **8**, 5364–5374; (c) A. Dutt, M. G. B. Drew and A. Pramanik, *Org. Biomol. Chem.*, 2005, **3**, 2250–2254.
- 15 (a) P. G. Vasudev, K. Ananda, S. Chatterjee, S. Aravinda, N. Shamala and P. Balaram, *J. Am. Chem. Soc.*, 2007, **129**, 4039–4048; (b) P. G. Vasudev, S. Chatterjee, K. Ananda, N. Shamala and P. Balaram, *Angew. Chem., Int. Ed.*, 2008, **47**, 6430–6432; (c) K. Ananda, P. G. Vasudev, A. Sengupta, K. M. P. Raja, N. Shamala and P. Balaram, *J. Am. Chem. Soc.*, 2005, **127**, 16668–16674.
- 16 (a) B. F. Fisher, L. Guo, B. S. Dolinar, I. A. Guzei and S. H. Gellman, *J. Am. Chem. Soc.*, 2015, **137**, 6484–6487; (b) M. W. Giuliano, S. J. Maynard, A. M. Almeida, L. Guo, I. A. Guzei, L. C. Spencer and S. H. Gellman, *J. Am. Chem. Soc.*, 2014, **136**, 15046–15053.
- 17 (a) J. B. Ghiara, E. A. Stura, R. L. Stanfield, A. T. Profy and I. A. Wilson, *Science*, 1994, **264**, 82–85; (b) J. M. Aizpurua, C. Palomo, E. Balentova, A. Jimenez, E. Andreieff, M. Sagartzazu-Aizpurua, J. I. Miranda and A. Linden, *J. Org. Chem.*, 2013, **78**, 224–237; (c) C. J. Saavedra, A. Boto, R. Hernandez, J. I. Miranda and J. M. Aizpurua, *J. Org. Chem.*, 2012, **77**, 5907–5913; (d) A. I. Jimenez, G. Ballano and C. Cativiela, *Angew. Chem., Int. Ed.*, 2005, **44**, 396–399; (e) S. Guha, M. G. B. Drew and A. Banerjee, *Tetrahedron Lett.*, 2006, **47**, 7951–7955; (f) S. K. Maji, R. Banerjee, D. Velmurugan, A. Razak, H. K. Fun and A. Banerjee, *J. Org. Chem.*, 2002, **67**, 633–639; (g) A. K. Das, A. Banerjee, M. G. B. Drew, S. Ray, D. Haldar and A. Banerjee, *Tetrahedron*, 2005, **61**, 5027–5036; (h) D. Srinivas, R. Gonnade, S. Ravindranathan and G. J. Sanjayana, *Tetrahedron*, 2006, **62**, 10141–10146.
- 18 (a) S. Aravinda, K. Ananda, N. Shamala and P. Balaram, *Chem. – Eur. J.*, 2003, **9**, 4789–4795; (b) K. Ananda, S. Aravinda, P. G. Vasudev, K. M. P. Raja, H. Sivaramakrishnan, K. Nagarajan, N. Shamala and P. Balaram, *Curr. Sci.*, 2003, **85**, 1002–1011; (c) I. O. Lebedyeva, D. A. Ostrov, J. Neubert, P. J. Steel, K. Patel, S. M. Sileno, K. Goncalves, M. A. Ibrahim, K. A. Alamry and A. R. Katritzky, *Bioorg. Med. Chem.*, 2014, **22**, 1479–1486.
- 19 (a) R. Kaul and P. Balaram, *Bioorg. Med. Chem.*, 1999, **7**, 105–117; (b) E. Benedetti, *Biopolymers*, 1996, **40**, 3–44; (c) C. Toniolo and E. Benedetti, *Macromolecules*, 1991, **24**, 4004–4009; (d) C. Toniolo, M. Crisma, F. Formaggio and C. Peggion, *Biopolymers*, 2001, **60**, 396–419.
- 20 R. Gessmann, H. Bruckner and K. J. Petratos, *Pept. Sci.*, 2003, **9**, 753–762.
- 21 (a) H. W. German, S. Uyaver and U. H. E. Hansmann, *J. Phys. Chem. A*, 2015, **119**, 1609–1615; (b) W. Liyanage and B. L. Nilsson, *Langmuir*, 2016, **32**, 787–799.
- 22 (a) M. C. Manning and R. W. Woody, *Biopolymers*, 1991, **31**, 569–586; (b) A. Chakrabarty, T. Kortemme, S. Padmanabhan and R. L. Baldwin, *Biochemistry*, 1993, **32**, 5560–5565; (c) E. Robert, T. Lefevre, M. Fillion, B. Martial, J. Dionne and M. Auger, *Biochemistry*, 2015, **54**, 3932–3941;
- (d) A. Gokhale, T. K. Weldeghiorghis, V. Taneja and S. D. Satyanarayanajois, *J. Med. Chem.*, 2011, **54**, 5307–5319; (e) R. W. Woody, in *The Peptides*, ed. S. Udenfriend, J. Meienhofer and J. R. Hruby, Academic Press, Orlando, FL, 1985, vol. 2, pp. 15–114.
- 23 (a) J. M. Lehn, *Science*, 2002, **295**, 2400–2403; (b) G. M. Whitesides and B. Grzybowski, *Science*, 2002, **295**, 2418–2421; (c) L. Fischer and G. Guichard, *Org. Biomol. Chem.*, 2010, **8**, 3101–3117.
- 24 (a) M. R. Ghadiri, J. R. Granja, R. A. Milligan, D. E. McRee and N. Khazanovich, *Nature*, 1993, **366**, 324–327; (b) R. J. Brea, C. Reiriz and J. R. Granja, *Chem. Soc. Rev.*, 2010, **39**, 1448–1456; (c) D. T. Bong, T. D. Clark, J. R. Granja and M. R. Ghadiri, *Angew. Chem., Int. Ed.*, 2001, **40**, 988–1011; (d) C. H. Gorbitz, *Chem. – Eur. J.*, 2001, **7**, 5153–5159.
- 25 (a) E. Gazit, *Chem. Soc. Rev.*, 2007, **36**, 1263–1269; (b) X. Yan, P. Zhu and J. Li, *Chem. Soc. Rev.*, 2010, **39**, 1877–1890; (c) V. Semetey, C. Didierjean, J. P. Briand, A. Aubry and G. Guichard, *Angew. Chem., Int. Ed.*, 2002, **41**, 1895–1898.
- 26 (a) J.-H. Eom, J. Gong, S. Kwon, A. Jeon, R. Jeong, R. W. Driver and H.-S. Lee, *Angew. Chem., Int. Ed.*, 2015, **54**, 13204–13207; (b) S. H. Yoo, T. Eom, S. Kwon, J. Gong, J. Kim, S. J. Cho, R. W. Driver, Y. Lee, H. Kim and H.-S. Lee, *J. Am. Chem. Soc.*, 2015, **137**, 2159–2162.
- 27 (a) W. Cai, G.-T. Wang, Y.-X. Xu, X.-K. Jiang and Z.-T. Li, *J. Am. Chem. Soc.*, 2008, **130**, 6936–6937; (b) Y.-X. Xu, G.-T. Wang, X. Zhao, X.-K. Jiang and Z.-T. Li, *Langmuir*, 2009, **25**, 2684–2688.
- 28 J. K. Lee and B. R. Lentz, *Biochemistry*, 1997, **36**, 6251–6259.
- 29 (a) J. Naskar and A. Banerjee, *Chem. – Asian J.*, 2009, **4**, 1817–1823; (b) S. Ghosh, M. Reches, E. Gazit and S. Verma, *Angew. Chem., Int. Ed.*, 2007, **46**, 2002–2004; (c) S. Ghosh, S. K. Singh and S. Verma, *Chem. Commun.*, 2007, 2296–2298.
- 30 (a) C. E. Dempsey and P. E. Mason, *J. Am. Chem. Soc.*, 2006, **128**, 2762–2763; (b) N. Zacharias and D. A. Dougherty, *Trends Pharmacol. Sci.*, 2002, **23**, 281–287; (c) S. C. Nanita and R. G. Cooks, *Angew. Chem., Int. Ed.*, 2006, **45**, 554–569; (d) M. Kunimura, S. Sakamoto and K. Yamaguchi, *Org. Lett.*, 2002, **4**, 347–350.
- 31 (a) P. P. Bose, A. K. Das, R. P. Hedge, N. Shamala and A. Banerjee, *Chem. Mater.*, 2007, **19**, 6150–6157; (b) I. Maity, H. S. Parmar, D. B. Rasale and A. K. Das, *J. Mater. Chem. B*, 2014, **2**, 5272–5279; (c) F. Versluis, I. Tomatsu, S. Kehr, C. Fregonese, A. W. J. W. Tepper, M. C. A. Stuart, B. J. Ravoo, R. I. Koning and A. Kros, *J. Am. Chem. Soc.*, 2009, **131**, 13186–13187; (d) D. Ke, C. Zhan, A. D. Q. Li and J. Yao, *Angew. Chem., Int. Ed.*, 2011, **50**, 3715–3719.
- 32 (a) X. Yan, Q. He, K. Wang, L. Duan, Y. Cui and J. Li, *Angew. Chem., Int. Ed.*, 2007, **46**, 2431–2434; (b) A. Ajayaghosh, P. Chithra and R. Varghese, *Angew. Chem., Int. Ed.*, 2007, **46**, 230–233.
- 33 (a) S. Mann, *Nat. Mater.*, 2009, **8**, 781–792; (b) S. Mann, *Nature*, 1988, **332**, 119–124; (c) M. Maas, P. Guo, M. Keeney, F. Yang, T. M. Hsu, G. G. Fuller, C. R. Martin and

- R. N. Zare, *Nano Lett.*, 2011, **11**, 1383–1388; (d) Y. Wang, L. Cao, S. Guan, G. Shi, Q. Luo, L. Miao, I. Thistlethwaite, Z. Huang, J. Xu and J. Liu, *J. Mater. Chem.*, 2012, **22**, 2575–2581; (e) J.-X. Wang, Q. Lei, G.-F. Luo, T.-T. Cai, J.-L. Li, S.-X. Cheng, R.-X. Zhuo and X.-Z. Zhang, *Langmuir*, 2013, **29**, 6996–7004; (f) J. Ryu, S.-W. Kim, K. Kang and C. B. Park, *Adv. Mater.*, 2010, **22**, 5537–5541; (g) J. Ryu, S.-W. Kim, K. Kang and C. B. Park, *ACS Nano*, 2010, **4**, 159–164.
- 34 S. Zhang, M. A. Greenfield, A. Mata, L. C. Palmer, R. Bitton, J. R. Mantei, C. Aparicio, M. O. de la Cruz and S. I. Stupp, *Nat. Mater.*, 2010, **9**, 594–601.
- 35 S. R. Diegelmann, N. Hartman, N. Markovic and J. D. Tovar, *J. Am. Chem. Soc.*, 2012, **134**, 2028–2031.
- 36 J. Hartgerink, E. Beniash and S. I. Stupp, *Science*, 2001, **294**, 1684–1688.
- 37 (a) F. J. M. Hoeben, P. Jonkheijm, E. W. Meijer and A. P. H. J. Schenning, *Chem. Rev.*, 2005, **105**, 1491–1546; (b) H. Cao, X. Zhu and M. Liu, *Angew. Chem., Int. Ed.*, 2013, **52**, 4122–4126.
- 38 (a) P. Zhu, X. Yan, Y. Su, Y. Yang and J. Li, *Chem. – Eur. J.*, 2010, **16**, 3176–3183; (b) T. O. Mason, D. Y. Chirgadze, A. Levin, L. A. Abramovich, E. Gazit, T. P. J. Knowles and A. K. Buell, *ACS Nano*, 2014, **8**, 1243–1253; (c) M. Konda, I. Maity, D. B. Rasale and A. K. Das, *ChemPlusChem*, 2014, **79**, 1482–1488.
- 39 (a) L. Fischer, P. Claudon, N. Pendem, E. Miclet, C. Didierjean, E. Ennifar and G. Guichard, *Angew. Chem., Int. Ed.*, 2010, **49**, 1067–1070; (b) A. K. Das, D. Haldar, R. P. Hegde, N. Shamala and A. Banerjee, *Chem. Commun.*, 2005, 1836–1838; (c) S. Guha, M. G. B. Drew and A. Banerjee, *Org. Lett.*, 2007, **9**, 1347–1350.
- 40 (a) D. W. Zhang, X. Zhao, J.-L. Hou and Z.-T. Li, *Chem. Rev.*, 2012, **112**, 5271–5316; (b) Y. Liu, J. Shen, C. Sun, C. Ren and H. Zeng, *J. Am. Chem. Soc.*, 2015, **137**, 12055–12063.
- 41 (a) G. M. Sheldrick, *Acta Crystallogr., Sect. A: Fundam. Crystallogr.*, 2008, **64**, 112–122; (b) G. M. Sheldrick, *Acta Crystallogr., Sect. A: Fundam. Crystallogr.*, 2015, **71**, 3–8.